Letter

Dynamics of topological defects after photoinduced melting of a charge density wave

Andrei E. Tarkhov [1,*] A. V. Rozhkov [2] and Boris V. Fine [3,†]
[1]*Division of Genetics, Department of Medicine, Brigham and Women's Hospital and Harvard Medical School, Boston, Massachusetts 02115, USA*
[2]*Institute for Theoretical and Applied Electrodynamics, Russian Academy of Sciences, Moscow 125412, Russia*
[3]*Institute for Theoretical Physics, University of Leipzig, Brüderstr. 16, 04103 Leipzig, Germany*

(Received 8 March 2022; revised 2 August 2022; accepted 1 September 2022; published 20 September 2022)

Charge-density-wave order in a solid can be temporarily "melted" by a strong laser pulse. Here, we use the discrete Gross-Pitaevskii equation on a cubic lattice to simulate the recovery of the CDW long-range phase coherence following such a pulse. Our simulations indicate that the recovery process is dramatically slowed down by the three-dimensional topological defects—CDW dislocations—created as a result of strongly nonequilibrium heating and cooling of the system. Overall, the simulated CDW recovery was found to be remarkably reminiscent of a recent pump-probe experiment in $LaTe_3$.

DOI: 10.1103/PhysRevB.106.L121109

Topological defects in the form of vortices play a prominent role in nonequilibrium and equilibrium statistical physics of ordered systems [1–13]. In particular, vortices are known to emerge through the Kibble-Zurek mechanism [14–17], when the system is cooled across a phase transition. In the Kibble-Zurek setting, the system is initially at equilibrium, and the cooling process is supposed to be adiabatic everywhere except for a close vicinity of the phase transition temperature. It is still an outstanding question: What happens after a quench across a phase transition, where the initial state is far from equilibrium, and the energy flow from the system is so fast that the system does not reach quasiequilibrium at any time during the quench?

In the present Letter, we address the above question in the context of the recent pump-probe experiment of Ref. [18] on the light-induced melting of a charge density wave (CDW) in $LaTe_3$. The experiment monitored the recovery of the CDW order after its destruction by a laser pulse. The experimental system was initially in a low-temperature ordered phase; then the part of the system responsible for the CDW order was rapidly heated up and cooled down, so that it did not have time to reach the high-temperature equilibrium. It was observed [18] that the amplitude and the phase of the CDW responded qualitatively differently: The amplitude recovered quickly, whereas for sufficiently high pump pulse intensity, the recovery of phase coherence took much longer [19]. It was conjectured in Ref. [18] on the basis of indirect experimental evidence that the observed slowdown of the CDW order recovery is due to the slow dynamics of the photoinduced topological defects—CDW dislocations. Topological defects within the CDW phase were also invoked in other contexts in Refs. [20–27].

The translational symmetry breaking associated with the onset of a CDW can be equivalently viewed as the breaking of the $U(1)$ symmetry with respect to the phase of the CDW order parameter. In such a picture, the CDW dislocations are mapped onto vortices in the underlying $U(1)$-ordered state (see Fig. 1).

In the present Letter, we simulate the principal features of the CDW phase dynamics with the help of the discrete Gross-Pitaevskii equation (DGPE), which also exhibits a $U(1)$ phase transition. We implement the heating-cooling quench, perform the numerical imaging of vortices, trace their dynamics, and thereby demonstrate that they are responsible for the slowdown of the order parameter recovery. The basic character of our simulations suggest that the observed nonequilibrium phenomenology is applicable to a broad class of physical systems.

General considerations. CDW is a modulation of electronic charge density accompanied by a periodic modulation of ionic positions

$$\mathbf{r}_m \rightarrow \mathbf{r}_m + u\,\mathbf{e}\cos\left(\mathbf{q}_{\mathrm{CDW}}\mathbf{r}_m + \phi\right), \tag{1}$$

where $\mathbf{r}_m$ is the position of the mth ion, $\mathbf{q}_{\mathrm{CDW}}$ the CDW wave vector, u and ϕ the amplitude and the phase of the CDW, and $\mathbf{e}$ the unit vector along the CDW lattice displacement direction [19]. One can choose the complex number $u\exp(i\phi)$ as the CDW order parameter. By allowing this order parameter to vary slowly in space and time, $u(\mathbf{r},t)\exp[i\phi(\mathbf{r},t)]$, one can then describe the low-frequency dynamics of a CDW.

In Fig. 2(a), we reproduce one of the experimental results of Ref. [18], namely, the time dependence of the two-dimensional (2D)-integrated intensity of the CDW diffraction peak for different fluences of the laser pump pulse. This intensity is proportional to the squared amplitude of the CDW order parameter. For smaller pulse fluences, the order parameter initially becomes smaller but never vanishes entirely and then quickly recovers to almost the initial value. For higher fluences, the CDW first disappears, i.e., becomes totally melted, but then it recovers over much longer times, in fact, not reaching the equilibrium value on the timescale accessible in the experiment. The subsequent theoretical analysis

*atarkhov@bwh.harvard.edu
†boris.fine@uni-leipzig.de

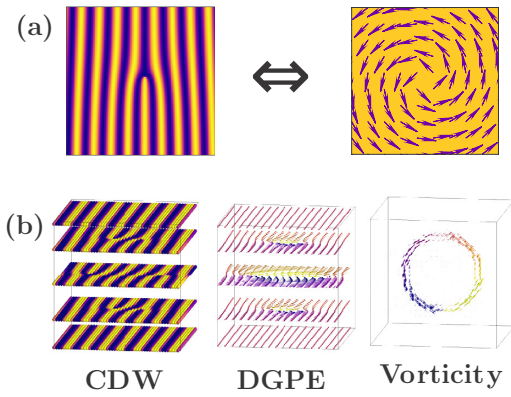

FIG. 1. Sketch of the mapping of a CDW dislocation $u\cos[\mathbf{q}_{\rm CDW}\mathbf{r}_m + \phi(\mathbf{r}_m)]$ onto a vortex of the DGPE $U(1)$ lattice variables $u\exp[i\phi(\mathbf{r}_m)]$. (a) 2D slice of the CDW dislocation (left) vs 2D slice of the DGPE vortex (right). (b) Three-dimensional representations of a vortex loop: CDW (left) vs DGPE lattice (middle) vs vorticity of the DGPE lattice defined in the text (right).

of Ref. [19] concluded that the above slow recovery cannot be explained by the amplitude dynamics of the CDW order (see also Refs. [28,29]). The amplitude takes about 2 ps to

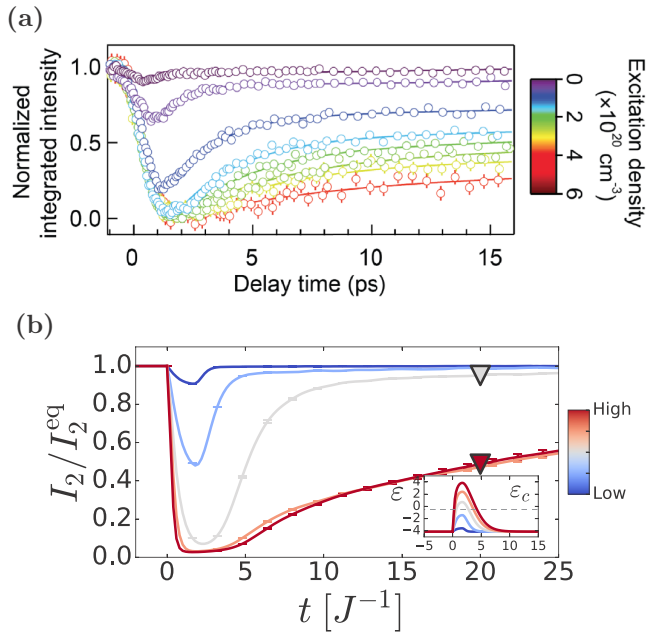

FIG. 2. (a) Time evolution of experimentally measured 2D-integrated intensity of the CDW electron diffraction peak after photoexcitation, for several laser photoexcitation densities (from Ref. [18]). (b) Numerically calculated 2D-integrated intensity $I_2 \equiv \sum_{k_x,k_y} |\psi(k_x,k_y,0)|^2$ tracking the ordering in the system [see Eq. (6)] as a function of time for different quench intensities. The color of the curves encodes different quench intensities as indicated on the color bar. Each numerical data point represents the average of 40 quench realizations, and the error bars represent the statistical uncertainty associated with this average. Inset: Variation of the energy density during quenches. The horizontal line marks the critical energy density ε_c [see Fig. 3(a)] above which the order is destroyed.

relax [18,19] It is the phase relaxation happening afterwards that we aim at describing in this Letter.

The model. Our numerical model, DGPE, is a space-discretized version of the continuous Gross-Pitaevskii equation (GPE). Both can be considered as possible dynamical extensions of the static XY model. The GPE describes the low-temperature dynamics of superfluid Bose gases, while the DGPE is often used to describe bosons on optical lattices. We note that both the spatially inhomogeneous CDW order $u(\mathbf{r})\exp[i\phi(\mathbf{r})]$ and the DGPE share the $U(1)$ structure of the dynamical variable, and both also exhibit a spontaneous symmetry breaking transition into a $U(1)$-ordered state. The actual dynamics of the inhomogeneous CDW is different and, in many respects, more complex than that of DGPE. Real CDWs are dissipatively coupled with the electrons and with the lattice degrees of freedom, while the DGPE dynamics is time reversible. Yet, due to the large number of degrees of freedom involved in the simulations, DGPE delivers an effectively dissipative environment for the smaller number of variables associated with the formation of topological defects over larger spatial scales. It can be reasonably expected that the detailed character of the thermal bath is not crucial here, and therefore the thermal bath of the real CDW system can be efficiently replaced by the bath associated with the microcanonical thermalizing dynamics of the DGPE lattice.

To connect the CDW dynamics and the DGPE, we divide the crystal lattice into cells of sizes $l_x \times l_y \times l_z$, where l_x, l_y, and l_z are of the order of the CDW coherence lengths for the respective directions. The mapping is achieved by associating the DGPE lattice variable ψ_j with the average of the CDW order parameter over the CDW cell around position $\mathbf{r}_j$:

$$\psi_j \sim \langle u(\mathbf{r})e^{i\phi(\mathbf{r})}\rangle_{j\text{th cell}}. \tag{2}$$

Given the crystal anisotropy of $LaTe_3$, the coherence length for the direction perpendicular to the Te layers, l_z, should be significantly smaller than l_x and l_y. We expect that l_x, l_y, and l_z can be chosen such that the renormalized phase stiffness between adjacent *anisotropic* unit cells can be modeled with the help of the same constant J [30–32] for all three directions. Each cell is thus represented by a single site of the cubic DGPE lattice. The modeling is classical, since, for large enough cells, the quantum fluctuations can be neglected.

The time evolution of ψ_j is to be modeled by the DGPE on a cubic lattice,

$$i\frac{d\psi_j}{dt} = -J\sum_{k\in \mathrm{NN}(j)}\psi_k + U|\psi_j|^2\psi_j, \tag{3}$$

where the summation over k runs through all nearest neighbors $\mathrm{NN}(j)$ of site j, coefficient J is the "hopping" parameter, and U is the interaction parameter. The lattice has V sites. In the simulations, the typical lattice dimensions were $50 \times 50 \times 50$. DGPE conserves the total energy of the lattice $E \equiv \sum_j(-J\sum_{k\in\mathrm{NN}(j)}\psi_k\psi_j^* + \frac{U}{2}|\psi_j|^4)$ as well as the "total norm" $N \equiv \sum_j |\psi_j|^2$. We also define the energy density $\varepsilon \equiv E/V - U/2$ and the "norm density" $n \equiv N/V$. The character of the DGPE solutions is determined by the dimensionless parameter $g \equiv Un/J$, which, for the reasons explained later, was chosen to be equal to 10. Below, except for the period of quench, we simulate an isolated DGPE lat-

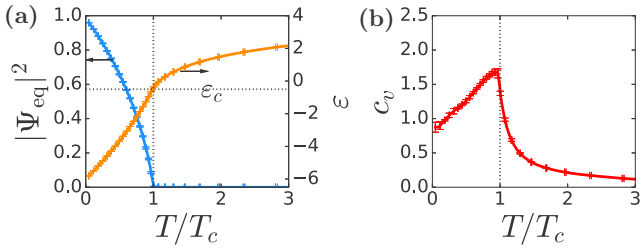

FIG. 3. Temperature dependence of various parameters for the 3D DGPE lattice: (a) The equilibrium order parameter $|\Psi_{eq}|^2$ and the energy density ε, and (b) specific heat c_v.

tice, which, when perturbed, is observed to exhibit dynamic thermalization [33,34] to a microcanonical temperature T that was determined numerically as in Refs. [35–38]. The computed temperature is a monotonic function of ε. For $g = 10, J = 1, n = 1$, the DGPE exhibits a spontaneous symmetry breaking transition at the critical temperature $T_c \approx 4.25$ into low-temperature ordered state characterized by the $U(1)$ order parameter $\Psi(t) = |\Psi(t)|e^{i\phi(t)} \equiv \frac{1}{\sqrt{nV}} \sum_j \psi_j(t)$. In equilibrium, $|\Psi| = |\Psi_{eq}|(T)$, where $|\Psi_{eq}|(T)$ is a decreasing function of T for $T < T_c$, vanishing above T_c. Both $\varepsilon(T)$ and $|\Psi_{eq}|^2(T)$ are plotted in Fig. 3(a). The heat capacity $c_v(T) \equiv d\varepsilon/dT$ is shown in Fig. 3(b); it exhibits a very recognizable cusp at $T = T_c$ corresponding to $\varepsilon = \varepsilon_c$.

In principle, Eq. (3) can be generalized to include disorder representing the CDW pinning centers. However, in the target experiment [18], the slowdown of the recovery of the CDW coherence was observed on the spatial scale where no evidence of the presence of the pinning centers was detected.

Parameters. To finalize the mapping, we provide the order-of-magnitude estimates for the three parameters of the cubic DGPE lattice, namely, J, n, and U.

Since the CDW coherent domains are supposed to be larger than the crystal unit cell, the CDW phase dynamics should occur at typical frequencies smaller than the Debye frequency Ω_D. Hence, the parameter J, which determines the characteristic frequency of the DGPE dynamics, can be roughly estimated as

$$J = \Omega_D \frac{a}{l}, \tag{4}$$

where $a \equiv (a_x a_y a_z)^{1/3}$ and $l \equiv (l_x l_y l_z)^{1/3}$ are the geometrical averages of the crystal lattice periods a_x, a_y, a_z and the CDW coherence lengths l_x, l_y, l_z, respectively. We use the mean-field theory [39], which is supposed to be rather crude for $LaTe_3$, to make the order-of-magnitude estimate $l = \hbar v_F/(1.76\pi k_B T_c)$, where $v_F = 2\varepsilon_F/p_F$ is the Fermi velocity, and T_c is the CDW phase transition temperature. Thus $\varepsilon_F \approx 1.5$ eV [40], $p_F \approx \frac{3\pi}{8}\frac{\hbar}{a}$, $T_c \sim 700$ K. As a result, we get $l \sim 6a$. Inserting this together with $\Omega_D \sim 4$ THz into Eq. (4) gives $J \sim 4$ ps^{-1}.

The typical value for n can be derived from the fact that, at the critical temperature, the hopping energy is of order of the thermal energy $Jn \sim k_B T_c$. Thus

$$n \sim \frac{k_B T_c}{J} \sim \hbar \frac{T_c}{T_D}\frac{l}{a}. \tag{5}$$

At the last step, we replaced $\hbar\Omega_D$ in Eq. (4) with $k_B T_D$, where $T_D \sim 200$ K is the Debye temperature for $LaTe_3$ [41]. Thus $n/\hbar \sim 20$, which is consistent with the classical character of our modeling.

Parameter U can be determined by matching the speed of phasons c_{ph} with the speed of low-frequency excitations of the DGPE lattice: $c_{ph} = l\sqrt{2JUn}$ [32]. In turn, c_{ph} can be crudely estimated as the speed of sound [42]. It is further shown in the Supplemental Material [32] that, under these assumptions, $U \sim 10\frac{J}{n}$. Therefore, our simulations were done with $g = Un/J = 10$.

Simulations of nonequilibrium quenches. According to Ref. [19], the energy deposited by the laser pulse into $LaTe_3$ is first absorbed by the electrons, then transferred partially to the "hot phonons," drastically increasing their temperature and thereby melting the CDW order. After that, the energy of the hot phonons is transferred to the rest of the phonons, which have significantly larger specific heat. This brings the overall temperature of the system to nearly the same temperature as the one before the pulse. The phase degrees of freedom we aim at describing with the help of the DGPE are supposed to belong to hot phonons. We model the above process by first quickly pumping the energy into the DGPE lattice (heating of hot phonons by electrons) and then quickly removing the energy from the lattice (cooling of hot phonons by the energy transfer to the main phonon bath). Technically the above scheme is implemented by temporarily adding the energy-nonconserving terms to the right-hand side of Eq. (3) as explained in Refs. [32,36,43,44].

We simulated a set of quenches starting from the equilibrium state at $T \approx 0.4T_c$ and then using varying amounts of energy deposited to and then removed from the system, and averaged over 40 random initial conditions, thermalized before the quench for $t = 600J^{-1}$ [32]. The time dependencies of energy during the quenches are shown in the inset of Fig. 2(b). These quenches imitated the experimental laser pulses of different fluences used to produce the experimental plots in Fig. 2(a).

To compare our simulation with the diffraction experiment [18], we define the two-dimensional integrated spectral weight $I_2(t)$ by the following equality,

$$I_2 = \sum_{k_x,k_y} |\psi(k_x, k_y, 0)|^2, \tag{6}$$

where $\psi(\mathbf{k}) = V^{-1} \sum_j \psi_j e^{i\mathbf{k}\cdot\mathbf{r}_j}$ is the Fourier transform of ψ_j. Summation in Eq. (6) runs over quantized momentum projections $k_{x,y}$ lying in the Brillouin zone, while $k_z = 0$. Definition (6) mimics the 2D-integrated diffraction intensity measured experimentally in Ref. [18] [see Fig. 2(a)]. The square of the order parameter amplitude $|\Psi|^2$ is the largest contributing term in the sum (6). However, $I_2 > |\Psi|^2$ since shorter-range order fluctuations enhance I_2 relative to $|\Psi|^2$. Thus, one can think of I_2 as a quantity tracking both long-range and short-range correlations in the DGPE system. We have further verified [32] that $I_2(t)$ is proportional to the correlation length of the CDW order, $l_c(t)$, as anticipated in Refs. [18,19].

The main panel of Fig. 2(b) presents $I_2(t)$ before, during, and after the quench. The comparison between the simulation and the experiment reveals a remarkable agreement: At small intensities of the quench, the spectral intensity

quickly recovers its prequench equilibrium value on the timescale comparable to the duration of the quench itself. As the quench intensity grows, the character of the dynamics undergoes a qualitative change: I_2 drops to zero and stays low for a finite time interval. This happens when, during the quench, the energy crosses the critical value ε_c associated with the phase transition and indicated by the dashed line in the inset of Fig. 2(b). Most importantly, the postquench recovery is extremely slow: The corresponding curves visually split away from the curves representing weaker quenches.

Topological defects. Here, we investigate the possible connection between the slowdown of the order recovery and the dynamics of topological defects. For 3D DGPE systems with periodic boundary conditions, the topological defects form closed-loop vortices [45]. In this respect, the 3D DGPE model is similar to the three-dimensional $O(2)$, $U(1)$, and XY models, where the percolation of vortex loops is responsible for a phase transition [46–48].

To monitor the local topological charge (vorticity), we define the dual lattice by translating the original lattice by vector $(1/2, 1/2, 1/2)$. Each of the sites of the dual lattice is thus surrounded by six square plaquettes of the original lattice.

As an indicator of vorticity we use the finite-difference counterpart $\mathbf{w}_j$ of the continuous curl of the current $(\nabla \times \mathbf{v}_s)_j$, where $\mathbf{v}_s = -i(\psi^*\nabla\psi - \psi\nabla\psi^*)$ (see Supplemental Material [32]). In Figs. 4(a) and 4(b), we provide a space-resolved snapshots of field $\mathbf{w}_j$ generated in the course of the quenches shown in Fig. 2(b). The snapshots correspond to the two states marked in Fig. 2(b) by red and gray triangles. In principle, each site of the dual lattice has a nonzero vorticity $\mathbf{w}_j$, which is the consequence of the discreteness of the lattice field. However, in the absence of a real vortex, such a vorticity is very small and does not form any line pattern, while the presence of a vortex is indicated by the large values of $\mathbf{w}_j$ showing the vortex core as a colored "tube" extended through the lattice.

Figure 4(a) illustrates a weak quench, for which the order (quantified by I_2) recovers quickly. One can see that the system does not exhibit any colored tube indicative of a vortex. For more intensive quenches, on the contrary, one can observe vortex tubes percolating through large volumes of the system and forming clearly identifiable large vortex loops [see Fig. 4(b)] [see also Figs. S7(a)–S7(c) and the video in the Supplemental Material [32]]. As one can see, for example, in the video, these loops initially form an entangled network. The crossings of the loop lines then lead to smaller loops separating from this network and collapsing, while one large loop spreading over most of the lattice is eventually being formed. The time required for that last loop to shrink and collapse is what determines the timescale of the order recovery in Fig. 2(b).

We also introduce an auxiliary binary vorticity variable Q_j for each dual lattice site [32]: It is defined such that $Q_j = 1$, if at least one of the six adjacent original-lattice plaquettes has nonzero vorticity; otherwise $Q_j = 0$. Finally, we define the average vorticity for the entire system as $Q_{\rm av} = \frac{1}{V}\sum_j^V Q_j$.

Further evidence that the relaxation of vorticity $Q_{\rm av}(t)$ is directly correlated with the order recovery after a quench is presented in Figs. 4(c) and 4(d): There the strong quenches exhibiting the slowdown of the I_2 recovery are accompanied by pronounced slowly relaxing tails of $Q_{\rm av}(t)$.

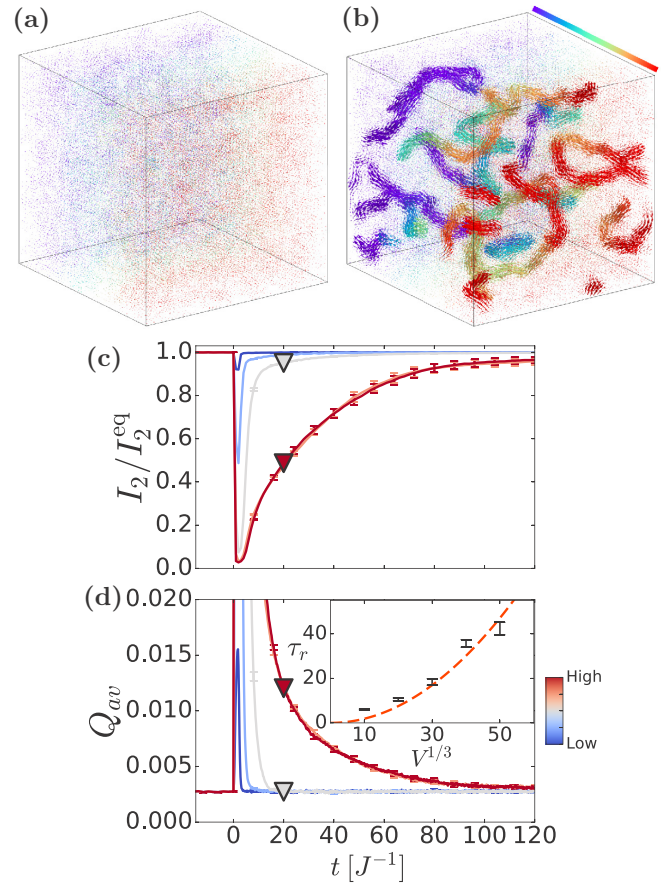

FIG. 4. (a), (b) Snapshots of vorticity for two individual quenches at time $t = 20J^{-1}$: (a) weak quench, (b) strong quench, marked in (c) and (d) by gray and red triangles, respectively [also shown in Fig. 2(b)]. Vorticity $\mathbf{w}_j$ is depicted by (colored) arrows whose length is proportional to $|\mathbf{w}_j|$ (see the text). For the visualization purposes, we apply a smoothing filter to $\mathbf{w}_j$: At site j we plot $\mathbf{w}_j$ averaged over 9 sites comprising a cube with side 3 encompassing site j. The arrow color represents the position along one of the lattice axes, as shown by the color bar. In (a) these arrows are visible as mere dots due to the smallness of $|\mathbf{w}_j|$. In (b) longer and hence brighter arrows merge into distinctly visible wormlike bundles revealing vortex cores. Vortex lines penetrating the entire system are clearly seen for the stronger quench. (Further snapshots of vorticity for the later times of the stronger quench can be found in the Supplemental Material [32].) (c), (d) Correlation between vorticity and the slowing down of the order recovery for the simulated 3D DGPE lattice. (c) The 2D-integrated intensity $I_2(t)$, same as Fig. 2(b) but over a longer time interval; (d) the average vorticity $Q_{\rm av}(t)$. The color coding and the statistical ensemble behind the sampling are used the same as in Fig. 2(b). (d) Inset: Dependence of the order parameter recovery time τ_r on the linear lattice size $V^{1/3}$.

In the inset in Fig. 4(c), we show that the order parameter recovery τ_r, defined as the time to reach 75% of the initial equilibrium value of $|\Psi|^2$ for the strongest quench, grows with the lattice volume (number of lattice sites) V. The simulations are consistent with the scaling $\tau_r \propto V^{2/3}$. We have not

attempted to derive this power law. Yet, the growth of τ_r with the lattice size as such indicates that the recovery of the order is contingent on the disappearance of the extensive vortex loops that penetrate the entire system and need to drift by the distances of the order of the lattice size before they annihilate.

Conclusions. In conclusion, our direct simulations of the DGPE lattice with a CDW-like form of the order parameter are consistent with the conjecture of Ref. [18] that the observed slowdown of the recovery of the CDW order after laser-induced melting is due to the emergence and then slow disappearance of topological defects in the order parameter texture. We were able to numerically monitor the vorticity in the system and thereby establish the correlation between the relaxation of vorticity and the recovery of the order. In a broader context, our investigation illustrates the viability of using DGPE for simulating the CDW dynamics even though DGPE as such was historically introduced to describe superfluid systems.

The source code is published in a GitHub repository [49].

This work was supported in part by a grant of the Russian Science Foundation (Project No. 17-12-01587).

[1] V. L. Berezinskii, Zh. Eksp. Teor. Fiz. **59**, 907 (1970) [Sov. Phys. JETP **32**, 493 (1971)].
[2] V. L. Berezinkskii, Zh. Eksp. Teor. Fiz. **61**, 1144 (1972) [Sov. Phys. JETP **34**, 610 (1972)].
[3] J. M. Kosterlitz and D. Thouless, J. Phys. C: Solid State Phys. **5**, L124 (1972).
[4] B. Svistunov, J. Moscow Phys. Soc **1**, 373 (1991).
[5] Yu. M. Kagan, B. V. Svistunov, and G. V. Shlyapnikov, Zh. Eksp. Teor. Fiz. **101**, 528 (1992) [Sov. Phys. JETP **74**, 279 (1992)].
[6] Yu. Kagan and B. V. Svistunov, Zh. Eksp. Teor. Fiz **105**, 353 (1994) [JETP **78**, 187 (1994)].
[7] N. G. Berloff and B. V. Svistunov, Phys. Rev. A **66**, 013603 (2002).
[8] H. Yoshino, K. Hukushima, and H. Takayama, Phys. Rev. B **66**, 064431 (2002).
[9] T. C. Proctor, D. A. Garanin, and E. M. Chudnovsky, Phys. Rev. Lett. **112**, 097201 (2014).
[10] D. A. Garanin and E. M. Chudnovsky, Eur. Phys. J. B **88**, 81 (2015).
[11] M. Kobayashi and L. F. Cugliandolo, Phys. Rev. E **94**, 062146 (2016).
[12] M. Kumar, S. Chatterjee, R. Paul, and S. Puri, Phys. Rev. E **96**, 042127 (2017).
[13] M. Vasin and V. Vinokur, Physica A **525**, 1161 (2019).
[14] T. W. Kibble, J. Phys. A: Math. Gen. **9**, 1387 (1976).
[15] T. W. Kibble, Phys. Rep. **67**, 183 (1980).
[16] W. H. Zurek, Nature (London) **317**, 505 (1985).
[17] W. H. Zurek, Phys. Rep. **276**, 177 (1996).
[18] A. Zong, A. Kogar, Y.-Q. Bie, T. Rohwer, C. Lee, E. Baldini, E. Ergeçen, M. B. Yilmaz, B. Freelon, E. J. Sie, H. Zhou, J. Straquadine, P. Walmsley, P. E. Dolgirev, A. V. Rozhkov, I. R. Fisher, P. Jarillo-Herrero, B. V. Fine, and N. Gedik, Nat. Phys. **15**, 27 (2019).
[19] P. E. Dolgirev, A. V. Rozhkov, A. Zong, A. Kogar, N. Gedik, and B. V. Fine, Phys. Rev. B **101**, 054203 (2020).
[20] M. Trigo, P. Giraldo-Gallo, J. N. Clark, M. E. Kozina, T. Henighan, M. P. Jiang, M. Chollet, I. R. Fisher, J. M. Glownia, T. Katayama, P. S. Kirchmann, D. Leuenberger, H. Liu, D. A. Reis, Z. X. Shen, and D. Zhu, Phys. Rev. B **103**, 054109 (2021).
[21] S. Wandel, F. Boschini, E. H. da Silva Neto, L. Shen, M. X. Na, S. Zohar, Y. Wang, G. B. Welch, M. H. Seaberg, J. D. Koralek, G. L. Dakovski, W. Hettel, M.-F. Lin, S. P. Moeller, W. F. Schlotter, A. H. Reid, M. P. Minitti, T. Boyle, F. He, R. Sutarto *et al.*, Science **376**, 860 (2022).
[22] A. Kogar, A. Zong, P. E. Dolgirev, X. Shen, J. Straquadine, Y.-Q. Bie, X. Wang, T. Rohwer, I.-C. Tung, Y. Yang, R. Li, J. Yang, S. Weathersby, S. Park, M. E. Kozina, E. J. Sie, H. Wen, P. Jarillo-Herrero, I. R. Fisher, X. Wang *et al.*, Nat. Phys. **16**, 159 (2020).
[23] D. Mihailovic, Appl. Sci. **9**, 890 (2019).
[24] S. Vogelgesang, G. Storeck, J. Horstmann, T. Diekmann, M. Sivis, S. Schramm, K. Rossnagel, S. Schäfer, and C. Ropers, Nat. Phys. **14**, 184 (2018).
[25] S. Duan, Y. Cheng, W. Xia, Y. Yang, C. Xu, F. Qi, C. Huang, T. Tang, Y. Guo, W. Luo *et al.*, Nature (London) **595**, 239 (2021).
[26] G. Storeck, J. G. Horstmann, T. Diekmann, S. Vogelgesang, G. von Witte, S. V. Yalunin, K. Rossnagel, and C. Ropers, Struct. Dyn. **7**, 034304 (2020).
[27] A. Zong, A. Kogar, and N. Gedik, MRS Bull. **46**, 720 (2021).
[28] J. Maklar, Y. W. Windsor, C. W. Nicholson, M. Puppin, P. Walmsley, V. Esposito, M. Porer, J. Rittmann, D. Leuenberger, M. Kubli, M. Savoini, E. Abreu, S. L. Johnson, P. Beaud, G. Ingold, U. Staub, I. R. Fisher, R. Ernstorfer, M. Wolf, and L. Rettig, Nat. Commun. **12**, 2499 (2021).
[29] A. Zong, P. E. Dolgirev, A. Kogar, E. Ergeçen, M. B. Yilmaz, Y.-Q. Bie, T. Rohwer, I. Cheng Tung, J. Straquadine, X. Wang, Y. Yang, X. Shen, R. Li, J. Yang, S. Park, M. C. Hoffmann, B. K. Ofori-Okai, M. E. Kozina, H. Wen, X. Wang *et al.*, Phys. Rev. Lett. **123**, 097601 (2019).
[30] J. Cardy, *Scaling and Renormalization in Statistical Physics*, Vol. 5 (Cambridge University Press, Cambridge, U.K., 1996).
[31] E. W. Carlson, S. A. Kivelson, V. J. Emery, and E. Manousakis, Phys. Rev. Lett. **83**, 612 (1999).
[32] See Supplemental Material at http://link.aps.org/supplemental/10.1103/PhysRevB.106.L121109 for details of the experiment; microcanonical thermodynamics of the DGPE lattice numerical aspects; numerical implementation of the DGPE lattice quench; estimate of parameter U for the DGPE lattice; definition of the vorticity characteristics; relation between I_2 and the correlation length of the CDW order; additional snapshots of vorticity after a quench; and simulations of anisotropic DGPE lattices.
[33] A. E. Tarkhov, S. Wimberger, and B. V. Fine, Phys. Rev. A **96**, 023624 (2017).
[34] A. E. Tarkhov and B. V. Fine, New J. Phys. **20**, 123021 (2018).
[35] A. S. de Wijn, B. Hess, and B. V. Fine, Phys. Rev. E **92**, 062929 (2015).
[36] A. E. Tarkhov, Ergodization dynamics of the Gross-Pitaevskii equation on a lattice, Ph.D. thesis, Skolkovo Institute of

Science and Technology, 2020, https://www.skoltech.ru/app/data/uploads/2020/10/thesis7.pdf.
[37] H. H. Rugh, Phys. Rev. Lett. **78**, 772 (1997).
[38] H. H. Rugh, J. Phys. A Math. Gen. **31**, 7761 (1998).
[39] G. Grüner, *Density Waves in Solids* (CRC Press, Boca Raton, FL, 2018).
[40] H. Yao, J. A. Robertson, E.-A. Kim, and S. A. Kivelson, Phys. Rev. B **74**, 245126 (2006).
[41] N. Ru and I. R. Fisher, Phys. Rev. B **73**, 033101 (2006).
[42] M. E. Manley, P. J. Stonaha, D. L. Abernathy, S. Chi, R. Sahul, R. P. Hermann, and J. D. Budai, Nat. Commun. **9**, 1823 (2018).
[43] A. E. Tarkhov, A. V. Rozhkov, and B. V. Fine, arXiv:2109.00961.
[44] A. Kamaletdinov and N. G. Berloff, arXiv:2109.05867.
[45] F. Rojas, S. Puri, and A. Bray, J. Phys. A: Math. Gen. **34**, 3985 (2001).
[46] A. Hulsebos, Nucl. Phys. B: Proc. Suppl. **34**, 695 (1994).
[47] K. Kajantie, M. Laine, T. Neuhaus, A. Rajantie, and K. Rummukainen, Phys. Lett. B **482**, 114 (2000).
[48] G. Kohring, R. E. Shrock, and P. Wills, Phys. Rev. Lett. **57**, 1358 (1986).
[49] The code is published in a GitHub repository at https://github.com/TarkhovAndrei/DGPE.